Analysis of Primex Targets

Covering the results of the sub-project XADDIFT

Philippe Martel

Rory Miskimen

University of Massachusetts
Amherst

October 2004

Introduction

An experiment to determine the lifetime of the neutral pion is scheduled to begin in the second half of 2004. This modern particle physics experiment, collaborated on by a multitude of groups working both in and out of Jefferson National Laboratories, is called Primex. This paper will discuss the work and results of three sub-projects, both studying the photon beam targets to be used in Primex. The first is an analysis of the density and thickness of the HOPG (Highly Ordered/Oriented Pyrolitic Graphite) targets. Second is a very similar analysis of the thickness of several Beryllium foils. The third, and more involved project, is XADDIFT (X-ray Attenuation Device for Determining Isotopic Foil Thickness), its goal being a high precision measurement of the thicknesses of two delicate metallic foils, one of lead, and one of tin.

Experiment background and goals

Previous experiments on the lifetime of the neutral pion have produced various results, the average of which agrees with the theoretical prediction. The uncertainty on this average, however, is almost three times the estimated error on the predicted value. Thus, one of the major goals of the Primex experiment is to produce a value for the lifetime with an uncertainty less than or equal to 1.4%, making it the most accurate experiment to date. Given an inherent uncertainty in the photon flux in the particle accelerator of about 1%, and the remaining large uncertainty being the target thickness, we see that the XADDIFT project needs to determine these thickness values to under 0.7% accuracy.

HOPG Targets

The HOPG targets were produced using high temperature (3273 K) Chemical Vapor Deposition (CVD) furnace technology. This process creates atomic layers of carbon oriented to each other in a crystalline form. A nice result of this process is the very low porosity of these blocks (1% as compared to normal graphite's 10% porosity). We had two nearly identical blocks about 380 mils thick, 5% radiation length, and one block about 77 mils thick, 1% radiation length, machined from a single block provided by SLAC from a previous experiment.

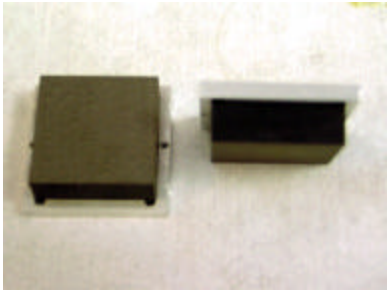

Figure 1 – HOPG targets

A piece of the block was sent away for an elemental analysis using two methods, Optimum Combustion Methodology (detects C, H, N, and O) and PIXE (Proton

Induced X-ray Emission, detects 72 elements).

Element	Abundance	Error (PIXE)
Carbon	99.63%	
Hydrogen	< 0.10%	
Nitrogen	< 0.05%	
Oxygen	0.19%	
Aluminum	0.00611%	0.00263%
Silicon	0.00568%	0.00144%
Chlorine	0.00285%	0.00067%
Calcium	0.00302%	0.00054%
Titanium	0.00037%	0.00017%
Vanadium	0.00079%	0.00011%
Chromium	0.00020%	0.00005%
Iron	0.00105%	0.00006%
Copper	0.00025%	0.00004%
Zinc	0.00033%	0.00005%

Table 1 – HOPG Composition

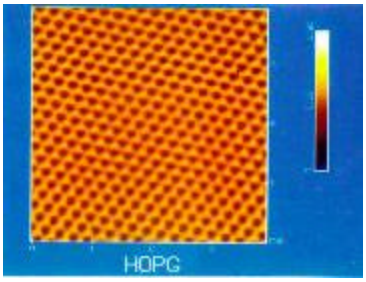

Figure 2 – Electron micrograph scan of HOPG surface

Thickness

A micrometer with a precision of ±0.05 mils is accurate enough for all of the targets, and perfectly suitable for the durable HOPG blocks. Two aluminum masks were machined with an array of holes drilled into them. Using these masks, in two different orientations each, provides a detailed map of the thickness.

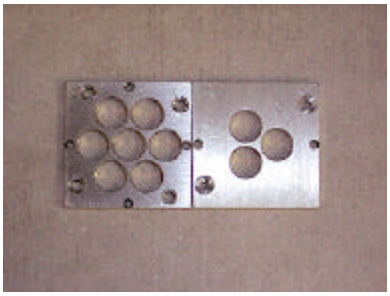

Figure 3 – HOPG micrometer masks

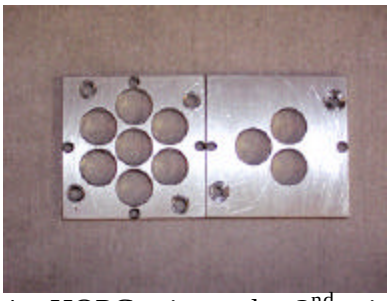

Figure 4 – HOPG mic masks, 2nd orientation

The frame for each block was marked in a corner with a roman numeral, so that identification of each, and orientation with regard to the masks (and the XADDIFT frame, as will be discussed later), is possible. The thickness values shown here are oriented with the identification mark visible in the upper-left hand corner. This notation is used throughout this paper, orienting the marking on each target to visibly be in the upper-left hand corner, regardless of how the micrometer masks are attached. This results in some careful data taking with regards to the other targets, as will be noted later.

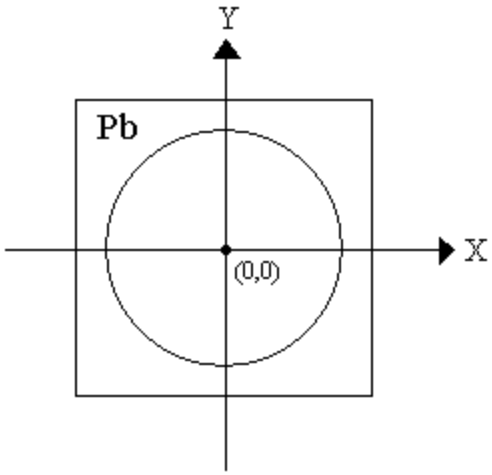

Figure 5 – Orientation of targets with regards to data

The Primex experiment at JLab makes use of a different orientation to that used here. The target is rotated clockwise by 90 degrees, with the identification mark then visible in the upper-right hand corner when viewing the target in the upstream (-z) direction. To match our coordinate system with the beam-line coordinate system, a simple transformation must be made:

$$\hat{x}_{Beam} = \hat{y} \qquad \text{Eq. 1}$$

$$\hat{y}_{Beam} = -\hat{x} \qquad \text{Eq. 2}$$

For the purposes of this paper, our *original orientation will be maintained*.

HOPG Target Thickness

Point	X (mils)	Y (mils)	Block I (mils)	Block II (mils)	Block III (mils)
1	-161.2	279.3	380.35	380.45	77.05
2	161.2	279.3	380.4	380.5	76.95
3	-322.5	0	380.2	380.5	76.75
4	0	0	380.35	380.4	76.95
5	322.5	0	380.35	380.25	76.75
6	-161.2	-279.3	380.2	380.45	76.7
7	161.2	-279.3	380.2	380.3	76.75
8	0	322.5	380.45	380.5	77.05
9	-279.3	161.2	380.3	380.5	76.9
10	279.3	161.2	380.4	380.3	76.95
11	0	0	380.35	380.4	76.85
12	-279.3	-161.2	380.15	380.5	76.75
13	279.3	-161.2	380.3	380.25	76.7
14	0	-322.5	380.25	380.4	76.75
15	-161.3	93.1	380.35	380.5	76.95
16	161.3	93.1	380.4	380.4	76.9
17	0	-186.2	380.25	380.55	76.8
18	0	186.2	380.45	380.5	76.95
19	-161.3	-93.1	380.25	380.5	76.8
20	161.3	-93.1	380.3	380.35	76.75

Table 2 - HOPG thickness measurements

Block I has a total variation of 0.3 mils, ±0.039%, from 380.15 to 380.45 mils. Block II also has a total variation of 0.3 mils, ±0.039%, however it ranges from 380.25 to 380.55 mils. Block III has a total variation of 0.35 mils, ±0.228%, from 76.70 to 77.05 mils.

Density

Using simple fluid mechanics, an easy method was devised to determine the actual density of the HOPG blocks. By comparing the mass of a block to its apparent mass in water, one can deduce the density of the block:

$$? = ?_{H_2O}\left(\frac{W_{air}}{W_{air} - W_{H_2O}}\right) \qquad \text{Eq. 3}$$

where ? is the density of the sample, $?_{H2O}$ is the density of the water, W_{air} is the weight of the sample in air, and W_{H2O} is the weight of the sample in water. Note that weight and mass are interchangeable in this instance, since the local acceleration due to gravity, g, can simply divide out. Since we're not examining the blocks mass, but rather the apparent weight, we shall stick to the term weight. The purity of the water is obviously very important, so we used HPLC Grade H_2O from Spectrum Chemical Mfg. Corp., which is Submicron Filtered, packed under Inert Gas, and has a maximum limit of impurities at 1 ppm. The apparatus for this consists of a milligram scale, a very accurate 10g test weight, a beaker, the water, and the setup to hang the block in the water without it touching the sides of the beaker. A thin wire frame goes around the beaker, suspending a small, spoon-like, holder in the beaker. The beaker itself is then held in the air by a clamp. This apparatus is shown here:

Figure 6 – Density, via water displacement, apparatus

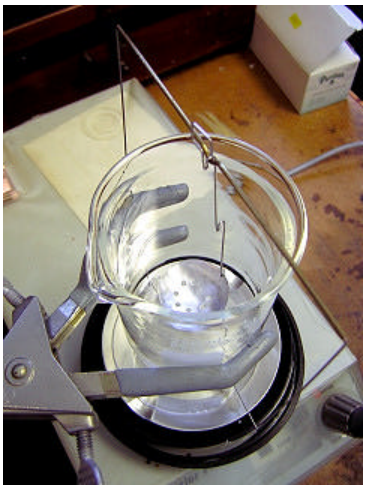

Figure 7 – HOPG holder suspended in beaker

After zeroing the scale, the 10g test weight was measured to check the scale. The apparatus, with the holder immersed in water, was then measured first without the block at all, then with the block on the beaker bottom (since a change in the water level should, and does, slightly affect the weight due to buoyancy), and finally with the block on the immersed holder. To double check these values, the experiment was backed up through each step, taking the average of each measurement as the needed value. Note that any bubbles on the target or apparatus while in the water, and any water droplets left on the tweezers can and will affect the results, so each step must be done carefully to avoid such problems. Each block was measured three separate times, each time noting the water temperature, since the density of water isn't exactly 1.

The following corrections were then made:

$$W_{air_{corrected}} = \overline{W_{air}} + \left(10 - \overline{W_{test}}\right) \qquad \text{Eq. 4}$$

$$W_{H_2O_{corrected}} = W_{H_2O} - \overline{W_{app}} \qquad \text{Eq. 5}$$

W_{air} is the average of the two measurements of the block in air, and W_{test} is the average of the test weight measurements (thus correcting for any deviation in the scale by comparing the measurement of the test weight to its known mass). W_{H2O} is the measurement of the block on the holder, and W_{app} is the average measurement of the apparatus with the block on the bottom of the beaker. The six measurements of density are shown in this figure/chart:

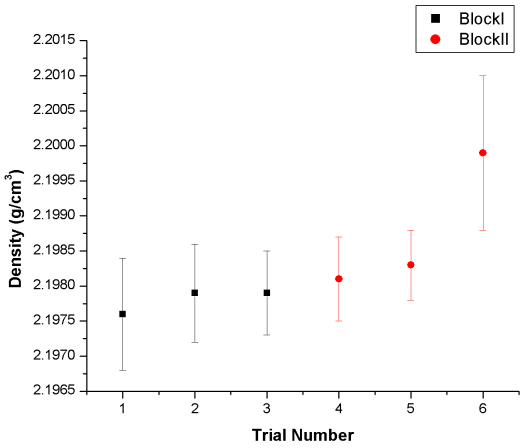

Figure 8 – HOPG density calculations

The average of these six values is 2.1983 ± 0.0002 g/cm^3, which is within the value provided with the blocks of 2.200 ± 0.002 g/cm^3. Even neglecting the questionable sixth point in the data, the average would be 2.1979 ± 0.0003 g/cm^3, which is still within error of the reported value.

Be Targets

The Be targets, while not being nearly as thick as the graphite blocks, are also considerably durable, thus the same method can be employed, though different aluminum masks were required, due to the different designs in the frames of the graphite and foil targets. Some care had to be taken in the handling of these foils, as Be is quite poisonous. Latex gloves and a painter's mask were used while manipulating these foils.

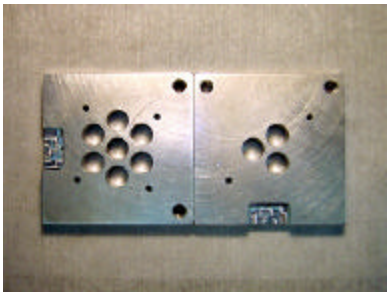

Figure 9 – Be mic masks

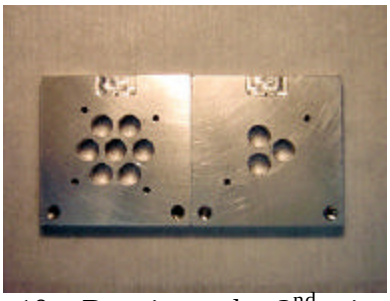

Figure 10 – Be mic masks, 2nd orientation

Be Target Thickness

Point	X (mils)	Y (mils)	Foil 1 (mils)	Foil 2 (mils)	Foil 3 (mils)	Foil 4 (mils)
1	-161.2	279.3	14.75	14.7	14.85	14.65
2	161.2	279.3	14.6	14.7	14.5	14.8
3	-322.5	0	14.65	14.7	15.2	14.5
4	0	0	14.6	14.7	14.9	14.7
5	322.5	0	14.6	14.75	14.5	14.7
6	-161.2	-279.3	14.7	14.65	14.95	14.7
7	161.2	-279.3	14.5	14.6	14.8	14.65
8	0	322.5	14.65	14.75	14.6	14.75
9	-279.3	161.2	14.7	14.7	14.6	14.55
10	279.3	161.2	14.55	14.75	14.45	14.75
11	0	0	14.55	14.7	14.7	14.7
12	-279.3	-161.2	14.6	14.65	14.6	14.6
13	279.3	-161.2	14.5	14.6	14.55	14.6
14	0	-322.5	14.4	14.7	14.7	14.6
15	93.1	161.3	14.65	14.7	14.6	14.8
16	-186.2	0	14.7	14.7	14.65	14.6
17	93.1	-161.3	14.55	14.65	14.8	14.7
18	-93.1	161.3	14.65	14.75	14.65	14.65
19	186.2	0	14.6	14.7	14.6	14.7
20	-93.1	-161.3	14.55	14.65	14.85	14.65

Table 3 – Thin Be targets, thickness measurements

Be Target Thickness

Point	X (mils)	Y (mils)	Foil 1 (mils)	Foil 2 (mils)	Foil 3 (mils)	Foil 4 (mils)
1	-161.2	279.3	70.5	70.3	70.7	70.75
2	161.2	279.3	70.35	69.95	70.65	70.7
3	-322.5	0	70.6	70.7	70.6	70.85
4	0	0	70.55	70.4	70.55	71
5	322.5	0	70.5	69.95	70.35	70.7
6	-161.2	-279.3	70.6	70.8	70.25	70.9
7	161.2	-279.3	70.7	70.25	70.1	70.9
8	0	322.5	70.35	70.1	70.7	70.7
9	-279.3	161.2	70.4	70.5	70.65	70.85
10	279.3	161.2	70.5	69.8	70.65	70.65
11	0	0	70.6	70.35	70.55	70.95
12	-279.3	-161.2	70.6	70.8	70.5	70.9
13	279.3	-161.2	70.55	69.95	70.25	70.8
14	0	-322.5	70.65	70.5	70.25	70.8
15	93.1	161.3	70.45	70.35	70.65	70.8
16	-186.2	0	70.55	70.65	70.55	70.8
17	93.1	-161.3	70.6	70.2	70.4	70.95
18	-93.1	161.3	70.4	70.4	70.75	71
19	186.2	0	70.5	70	70.4	70.9
20	-93.1	-161.3	70.55	70.6	70.35	70.9

Table 4 – Thick Be targets, thickness measurements

Targets two and five were chosen for having the smallest deviations of the thin and thick foils respectively. The thin foil is approximately 0.1% radiation length, while the thick foil is approximately 0.5% radiation length. It must be noted that the array of points does not completely match that of the HOPG targets. This is due to the orientation of the HOPG targets in the XADDIFT project, in which the 3-hole micrometer mask is rotated by 90 degrees.

Pb and Sn Targets

The other two foils are a ^{208}Pb foil of about 12 mils thickness, and a ^{120}Sn foil of about 23 mils thickness, both correspond to a 5% radiation length in the experiment. The foils are isotopically enriched with purities better than 98%. The reason for the exceptional purity of these foils is the simplification in the Primakoff reaction when the target nucleus has zero spin, and both of these elements have $J^p=0^+$. Considering the thin size and fragile nature of the foils, and their cost (purchased from Oak Ridge National Laboratory for $12.5k), a direct measurement posses the potential of 'dinging', denting, and/or compression of these delicate foils.

For this reason, an alternative method was devised, by which only four points would be physically measured with the micrometer. The attenuation of X-rays through the foils was then observed. X-ray attenuation is a well understood principle, in which the intensity of the beam is decreased exponentially by the thickness. By comparing the attenuation of x-rays through the foil at various points, the thickness at these points can be determined. The intensity is given by:

$$N(T) = N_0 e^{\frac{-T}{?}} \qquad \text{Eq. 6}$$

N_0 is the unattenuated intensity, T is the thickness, and ? is the x-ray attenuation length. This equation assumes a mono-energetic, perfectly collimated beam of particles travels through the attenuating matter to reach a detector that subtends zero solid angle. Secondary photons, scattered photons due to the Compton Effect, would therefore never be detected. This was considered to be an over-simplification of the problem, and it was determined that Compton scattered photons must be taken into account through a build up factor B(T,?), resulting in the following equation:

$$N(T) = N_0 B(T, ?) e^{\frac{-T}{?}} \qquad \text{Eq. 7}$$

It was found, through trials with various tin and lead foils of varying thickness, that this build-up factor can be characterized by the first order equation:

$$B(T, ?) = 1 + a\frac{T}{?} \qquad \text{Eq. 8}$$

where a is a material dependent constant. Higher orders were not found to affect the

calculations significantly, and are therefore omitted. Using each one of the four mic'd points as a calibration point, the value for a can be found by:

$$a = \frac{?}{T_C}\left(\frac{N_C}{N_0}e^{\frac{T_C}{?}} - 1\right) \qquad \text{Eq. 9}$$

where T_C is the measured thickness at the mic point, and N_C is the attenuated intensity at that point. The value of a can be averaged from the four calibration points.

Our ability to accurately determine the thickness is still rather limited with this method. Looking at the partial derivative equation for the thickness uncertainty, it was observed that the largest term is that associated with the uncertainty in lambda. This term itself, composed theoretically only of constants, results in an uncertainty of about 0.95% by itself. Without a better value for lambda, we obviously can't attain a successful value for the thickness. It can be shown that the build-up factor is indeed rather close to 1, since the aT/? value is approximately 0.0672 for lead, and 0.1453 for tin. The intensity can therefore be approximated using the exponential form initially used, greatly simplifying the equation. The methodology only slightly changes, where now we need to use the calibration (mic) points, to determine the value of the attenuation length, lambda, for each foil.

$$T = ?\ln\left(\frac{N0}{N}\right) \qquad \text{Eq. 10}$$

The values produced through this simplified process do agree rather well with the expected values for lambda. By approaching the problem this way, accuracies even better than expected are arrived upon. Further tests of this stability were done by repeating the measurements, instead at 100 mil step size. This repeats all the points previously measured, allowing for a check in reproducibility.

Apparatus setup

^{241}Am was the source chosen for our purpose, given its long half-life of 432 years, and the ease with which the 60 keV emission can be observed using a sodium iodide crystal attached to a photo-multiplier tube. The source is collimated using a 0.5" block of lead with a 1/16" (1.6 mm) diameter hole drilled through it. This is only slightly larger than the 1 mm diameter ^{241}Am bead. The source housing is also shielded by plates of lead to reduce x-ray emission to the rest of the room, and its occupants.

Figure 11 – ^{241}Am holder and collimator (pinhole in middle of top block)

The PMT with attached 1" cylindrical NaI crystal is hung above the collimator at the optimal height for maximizing signal intensity while limiting Compton scattered photons. This was achieved by determining the solid angle subtended by the source, assuming a point source, finding the height at which it achieved a 1" diameter circle, and setting the faceplate of the crystal there. By observing the signal strength in an oscilloscope at various heights, the legitimacy of this claim was shown.

A scanning platform was designed in order to facilitate very accurate placement of the target in the beam path. This platform uses two Hurst Mfg. Stepping Linear Actuators for movement in both the x and y directions. Such motion control via a LabVIEW program on the main computer, was tested and found to be accurate to within a mil. Control is run through a breakout box, designed and built by graduate student Eric Clinton, and is run by a Tektronix PS280 DC power supply.

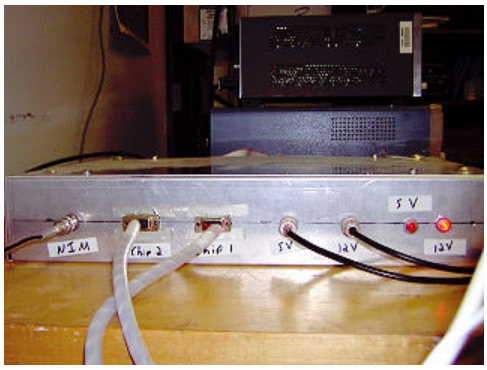

Figure 12 – Breakout box

The target frame, which rests upon this stepping platform, has three sections. The hole on the left always remains empty, and is used in the main program to look at N0, the no-absorber rate. The middle hole is the placeholder for the target, whose attachment will be described later. The hole on the right has two nails, approximately 75 mils in diameter, glued down, forming a crosshair used to produce a reference point for the experiment.

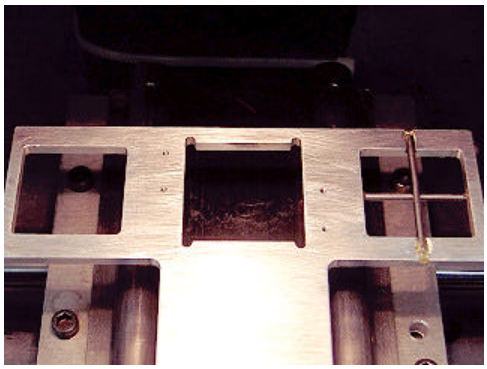

Figure 13 – Stepping motor frame

Initially this was the entire mechanical portion of the apparatus. Eventually it was determined that the background rate being observed by the NaI crystal was remarkably high, and due to its unstable nature our results had large uncertainties. Further analysis showed that the 60 keV peak sat directly upon the slope of the background signal. Any deviation in the background, taking into account its high count rate, could produce the sort of apparent gain-shifts in the 60 keV ADC spectrum. Since such deviations had been observed many times, in all of the various mechanical and electronic setups, the background became the prime focus.

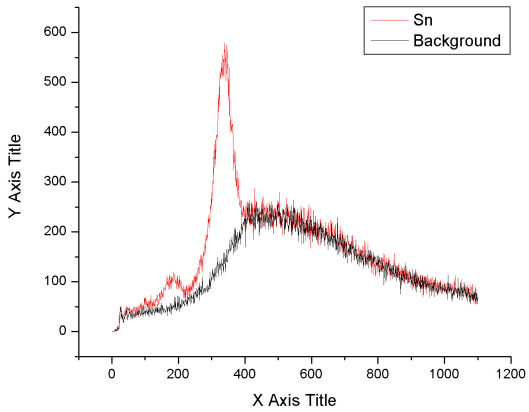

Figure 14 – Plot of ADC spectrum of Sn and background in old apparatus

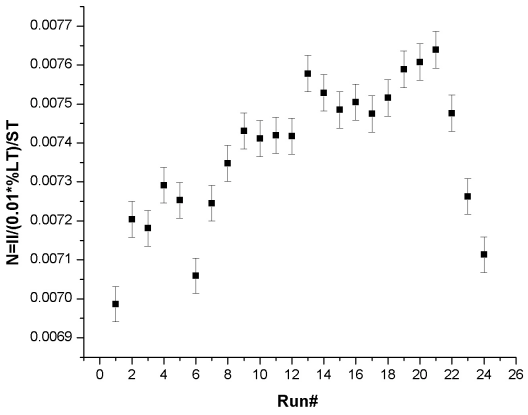

Figure 15 – Background fluctuation over a day

Methods to eliminate the background radiation, whose origins remain a mystery, were considered. Employing a 2 inch NaI crystal, a different PMT, and veto-counter paddles did little to improve the situation. A thick steel pipe was bought that would effectively shield the PMT from such a background. A reduction in this background rate of a factor of about 10 has allowed this experiment to proceed forward.

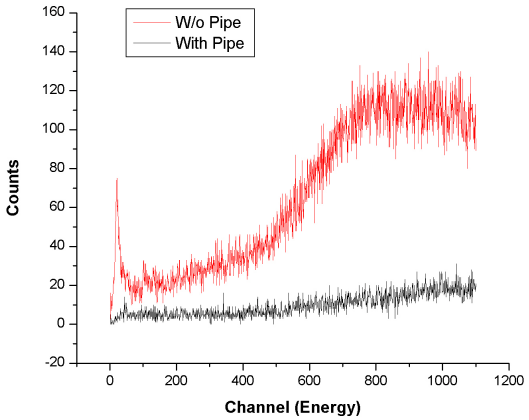

Figure 16 – Change in background signal with steel pipe in place

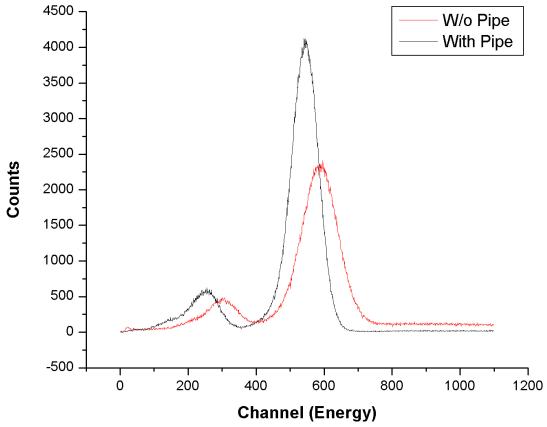

Figure 17 – Change in N0 ADC spectrum with pipe

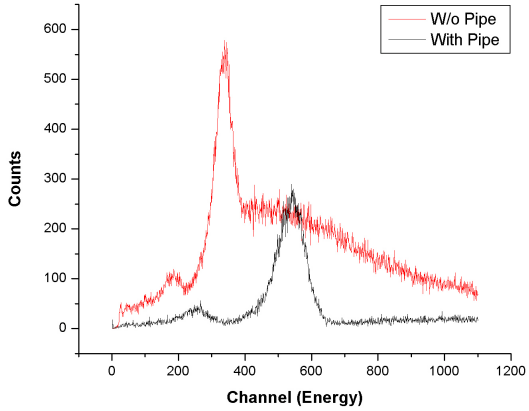

Figure 18 – Change in Sn ADC spectrum with pipe

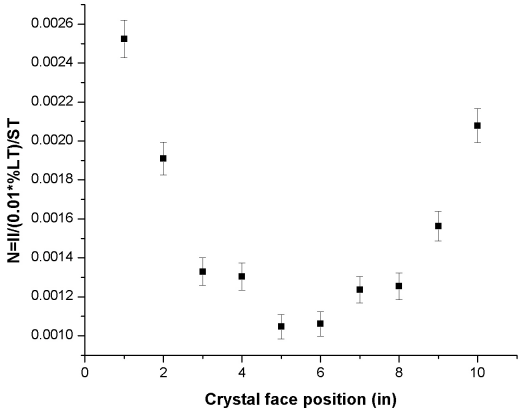

Figure 19 – Room background at various positions of the NaI detector within steel pipe

This pipe is aligned with the collimator using an aluminum plate, properly cut to just fit in the hole, with a pendulum hanging from the center. A simple test was run to determine the most effective position of the PMT within the pipe, the result being nearly in the center.

Figure 20 – Apparatus with steel pipe to decrease background radiation

The analog output of the PMT is then split by a 50O passive splitter, with one output sent through various time delays, both cable and box forms, and finally leading into a Camac module ADC (LeCroy model 2249A Analog-to-Digital Converter) after being AC coupled with 4000 pF capacitance. The ADC module returns an energy value of the input signal, which is binned in an 1100 element array. Thus, the ADC spectrum is a histogram with respect to channel number, or the energy of the observed signal. The other output from the splitter is amplified and integrated (100 ns) using a linear amplifier NIM module (Ortec model 410) to filter low energy noise from the detector. The signal is then checked by a discriminator NIM module (Phillips Scientific model 711), to determine valid signals. The output from the discriminator is a NIM level logic pulse. Two outputs from this module are used, both being identical pulse signals. One is read by a Camac scalar module (LeCroy model 2551) which simply counts the pulses, giving the total number of events that occur. The other discriminator output is used as the gating signal for the ADC. This is where the time delays employed for the analog signal come into play, as the gating signal must encompass the majority of the PMT signal. The width of the gating signal, set to 200 ns in this setup, can be specified through a potentiometer on the front panel of the discriminator, and calibrated by observing both the gate and PMT signals in an oscilloscope.

The timing of the runs is determined from a highly stable crystal oscillator, run through another channel of the discriminator. In order for the discriminator to fire on the TTL level signal, a 22 pF capacitor is used to differentiate the TTL pulse, the result being more than sufficient to be recognized as a valid pulse. The output from this

discriminator channel, about a 488 Hz NIM level pulse, is run into another scalar channel, to also be read by the computer.

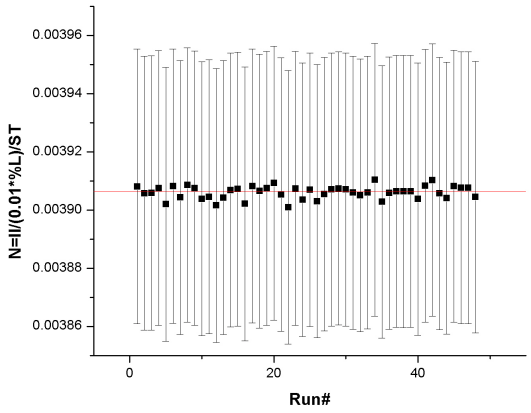

Figure 21 – Count rate check of crystal oscillator,
with expected value plotted as the red line

Final programs

The current programs in use by this experiment are Zerofinder 1.1, Stepping Pulse Generator 1.1, Data Collector 2.4 and 2.5, and XADDIFT Controller 1.5. The first two haven't been altered since I came on board. The latter two, however, have many changes to their operation. With the inclusion of the crystal oscillator as a clock, the program obviously had to be updated to make use of this device. The main changes in Data Collector 2.4 and 2.5 are in the data analysis section. Previous versions simply returned values for the integrated intensity, %livetime, and the time. The current versions allow for more detailed calculations, such as the average channel in the ADC spectrum, and the ability to save the data from a run in various files.

XADDIFT Controller 1.5 has many new items added to it, allowing one to specify whether or not, and the location, to save the data files. A greater range of step size has been implemented. Whereas before only certain step sizes were permitted, in order to assure that the mic points where x-rayed, this step is now taken separately, so that any integer length (in mils) can be specified. The ability to start up a run after total shutdown has been incorporated by requesting the starting point of the run. All four points have now been utilized in the Matlab script in the program, and correct values, including error analysis, is now given. A big change to this program is the ability to only run a portion of the program, either just looking at N0, the mic points, or the non-mic points of the target, looking at just the points on the target, doing a full run, or just performing the analysis (useful for changes in values, such as the integration limits, background rate, or mic-point thickness measurements). The program also only observes points within the target frame radius of 470 mils, to eliminate useless data points (and the waste of time such data taking accounts for). However, some extreme points may still be obviously incorrect, since the beam spot size is still finite.

XADDIFT Run

Before the scans took place, each foil had to be mic'd at the four points ((-220,-220);(220,-220);(-220,220);(220,220)), using a device designed to lessen the potential for damaging these delicate foils. By attaching the targets to the frame shown below, they can then be hung from a spring and directed into the micrometer head, which is held stationary by a clamp. The spring allows sufficient give in the position of the foil such that a very slow, and careful, approach can be made with the micrometer. It obviously is important that the points be recorded with regard to the inscription on the target frame, as shown.

Figure 22 – Micrometer setup

Figure 23 – Close up view of micrometer setup

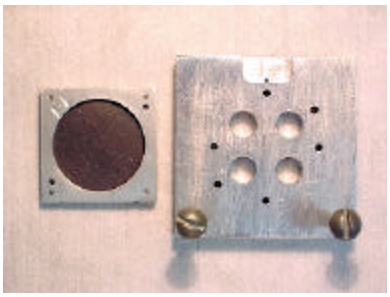

Figure 24 – Orientation of target with respect to mic frame

To begin a run, the chosen foil must be placed in the stepping motor frame. This is done by attaching the target foil to an aluminum faceplate, using two 0-80 screws. It's very important to orient the target as shown below, with the inscription of the target in the same corner as the faceplate 'up' inscription.

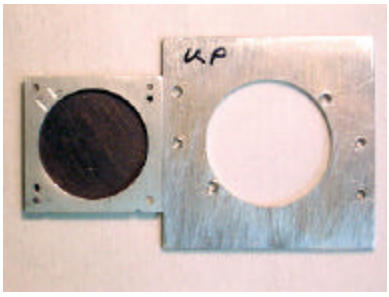

Figure 25 – Orientation of target with respect to scanning frame

Figure 26 – Foil target in scanning frame, with
Pb inscription barely visible in 'up' corner

For the HOPG targets, this is a bit tricky, as the blocks must be flipped in order to fit into their designated scanning frame. The block is oriented as shown in the following figure, and then flipped along the diagonal drawn through the 'I' notation corner, thus the 'I' notation is in the same corner as 'up', but on the opposite face (facing into the page). This must be kept in careful consideration when comparing the thickness data from the micrometer, as the data needs to be reflected across the diagonal noted.

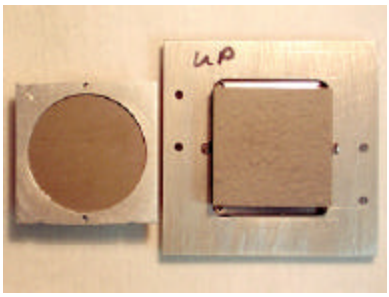

Figure 27 – HOPG target orientation with respect to scanning frame

This frame is then inserted into the middle section of the stepping motor frame, held down with four screws. The 'up' notation should read correctly by looking down at the apparatus as shown.

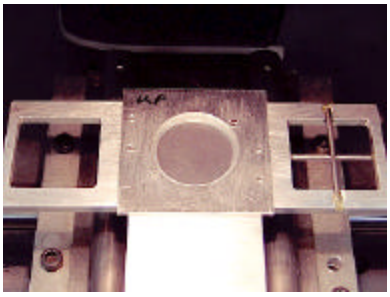

Figure 28 – Foil target placed in stepping motor frame

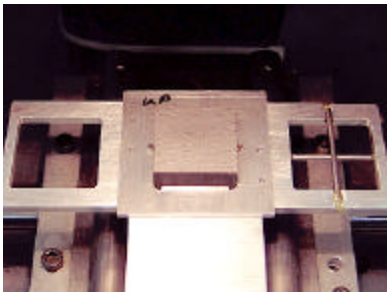

Figure 29 – HOPG target placed in stepping motor frame

Of important note is the fact that significant warm-up time is experienced in the electronics (almost exclusively in the PMT). Due to the significant effect that temperature changes have on a PMT, it is reasonable to conclude that thermal stability must be reached before attempting any runs. Several hours is a reasonable amount of time to allow for this, and in general the PMT remains on, even in the absence of a run taking place.

The setup must then be aligned for the zerofinder program. This is done manually using the Stepping Pulse Generator 1.1 program, and setting the collimator hole in the 'top-right' corner of the crosshair in the stepping motor frame. It should be placed about 50 mils off-center in each direction (unless the total scan of zerofinder is increased). The program then scans across (perpendicular to) each nail. By performing a Gaussian fit on this data curve, the center of the crosshair can be determined, and the program's reference point is set as such.

Figure 30 – Zerofinder setup, with collimator pinhole just visible in upper left hand corner of crosshair

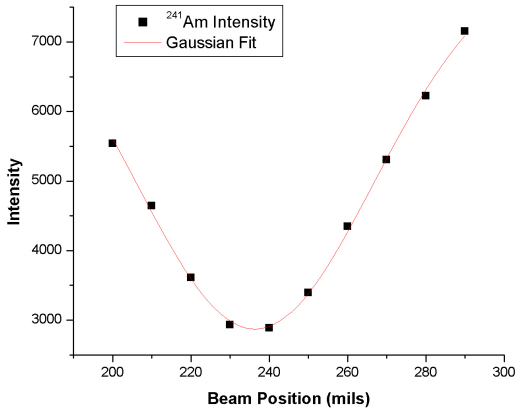

Figure 31 – Graph of Zerofinder data with Gaussian fit

The Camac crate has been a source of some difficulty during various runs, due to what is believed to be a charging/discharging capacitor in the crate. At seemingly random times, the crate will freeze up and discontinue communication with the computer. The programs have been altered to compensate for this, by sending an error message to the user, prompting for maintenance. Fixing this problem is done by shutting off the Camac crate, pausing for a minute or so, and then turning the crate back on. Once this is done, the dialog box button can be pressed, and the program will restart only the run that was interrupted.

Final Pb Data

Two runs were performed, a 200 mil step run, and a 100 mil step run.

Pb Target Thickness

X (mils)	Y (mils)	T (200 mil)	sT (200 mil)	T (100 mil)	sT (100 mil)
-200	-400	11.9291	0.0377	11.9766	0.0392
-100	-400			11.8306	0.0387
0	-400	11.8717	0.0375	11.8954	0.0389
100	-400			11.8273	0.0387
200	-400	11.8772	0.0375	11.9413	0.0391
-300	-300			11.8121	0.0387
-200	-300			11.9173	0.0390
-100	-300			11.9340	0.0391
0	-300			11.9439	0.0391
100	-300			11.9220	0.0390
200	-300			11.8864	0.0389
300	-300			11.6783	0.0383
-400	-200	11.8719	0.0375	11.9505	0.0391
-300	-200			11.8593	0.0388
-200	-200	11.9405	0.0377	11.9193	0.0390
-100	-200			12.0427	0.0394
0	-200	12.0278	0.0380	12.0557	0.0394
100	-200			12.0086	0.0393
200	-200	11.9206	0.0377	11.9203	0.0390
300	-200			11.8605	0.0388
400	-200	11.7982	0.0373	11.8447	0.0388
-400	-100			11.8398	0.0388
-300	-100			11.9084	0.0390
-200	-100			11.9760	0.0392
-100	-100			12.0671	0.0395
0	-100			12.0915	0.0396
100	-100			12.0563	0.0394
200	-100			11.9475	0.0391
300	-100			11.9210	0.0390
400	-100			11.7023	0.0383
-400	0	11.8359	0.0374	11.8284	0.0387
-300	0			11.9987	0.0393
-200	0	12.0623	0.0381	12.0772	0.0395
-100	0			12.0695	0.0395
0	0	12.0825	0.0381	12.0338	0.0394
100	0			11.9758	0.0392
200	0	11.9671	0.0378	11.9589	0.0391
300	0			11.8613	0.0388
400	0	11.6813	0.0370	11.6827	0.0383
-400	100			11.7523	0.0385
-300	100			11.9105	0.0390
-200	100			12.0505	0.0394
-100	100			12.0812	0.0395
0	100			12.0546	0.0394
100	100			11.9935	0.0393
200	100			12.0029	0.0393
300	100			11.8450	0.0388
400	100			11.6574	0.0382
-400	200	11.8916	0.0376	11.8497	0.0388
-300	200			11.7955	0.0386
-200	200	11.9177	0.0376	11.9257	0.0390
-100	200			11.9287	0.0391
0	200	11.9270	0.0377	11.9417	0.0391
100	200			11.9112	0.0390
200	200	11.8515	0.0375	11.8292	0.0388
300	200			11.7378	0.0385
400	200	11.8525	0.0375	11.7573	0.0385
-300	300			11.7742	0.0386
-200	300			11.7880	0.0386
-100	300			11.7889	0.0386
0	300			11.8539	0.0388
100	300			11.7673	0.0386
200	300			11.6724	0.0383
300	300			11.5707	0.0380
-200	400	11.9603	0.0378	11.8723	0.0389
-100	400			11.7255	0.0384
0	400	11.7213	0.0371	11.7060	0.0384
100	400			11.6967	0.0383
200	400	11.8687	0.0375	11.7625	0.0385

Table 5 – Pb Thickness values, 200 mil and 100 mil scans

The important points here are that most locations do agree, within error, between the 200 and 100 mil scans. The uncertainties on these points are approximately 0.038 mils, ±0.317%, which are more accurate than we could achieve with the micrometer. Some thought has been put into this concept, that data based upon a measurement can become more accurate than the measurement itself. Due to the nature of averaging the calculated values for lambda at the four mic points, we believe that this theory is reasonable. The lambda values at each of the mic points, for both scans, is shown here.

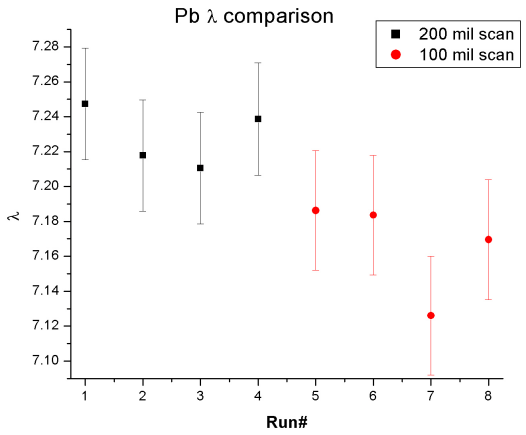

Figure 32 – Calculated lambda values for Pb

Using Matlab, the thickness values were plotted in a 3D form, to get a better grasp on the overall trends in the target.

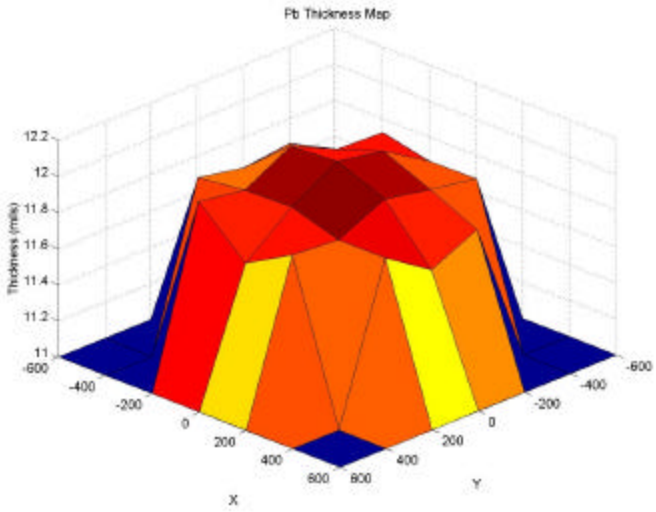

Figure 33 – Pb scan at 200 mils

The coarseness of this scan is clearly shown, considering there are only five observed points, in each direction, across the origin. However, the general trend of the foil is clear, with a peak in the middle becoming thinner as you move radially outward on

the foil. The finer scan should, and does, portray this same characteristic.

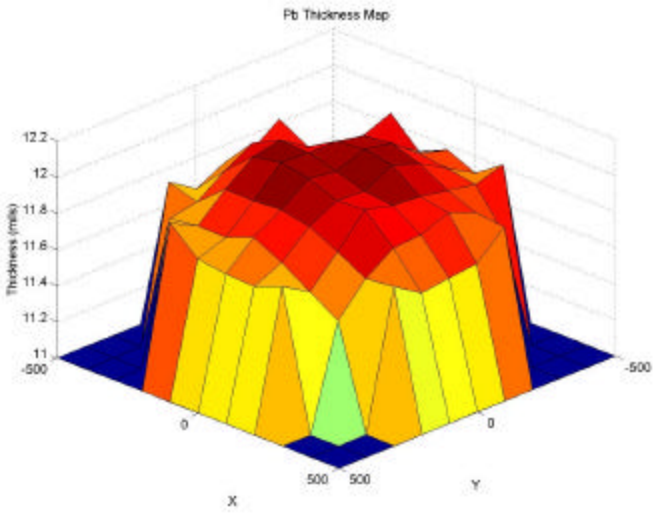

Figure 34 – Pb scan at 100 mils

Now the advantage of the 100 mil scan is very clear, with a much greater detailing of the shape of the Pb foil. The very center of the foil is just slightly thinner than the immediate vicinity, which forms more of a plateau than previously thought. One will note the very corners of this data as suddenly increasing in thickness. These values are most likely influenced from the target frame, as the beam spot size on the foil is only finitely small. As Primex is unlikely to use the extreme sections of the foil, these points are kept in the report as a reference, if nothing else.

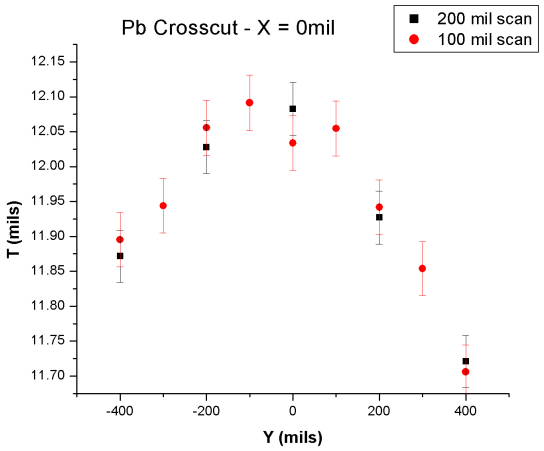

Figure 35 – Crosscut of Pb along Y axis

The most important points were deemed to be those along the two axes, crossing through the center. Those points along the Y axis are shown above, and it's clear from this plot that the two scans do agree quite well.

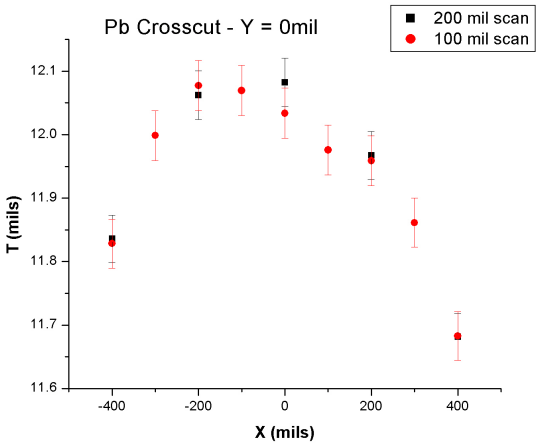

Figure 36 – Crosscut of Pb along X axis

Likewise, in the scans across the X axis as shown above, the points agree quite well. In fact, as can be seen in Table 5, all of the points, except for three, agree within error. The three points that don't agree are (400, 200), (-200, 400), and (200, 400). These points are among those mentioned before as the very corners of the foil, and therefore are going to be flawed to begin with, considering the slight attenuation from the neighboring aluminum frame.

Final Sn Data

The tin target has proved to be the more difficult to analyze, which is surprising considering that lead is a better attenuator. The tin target is almost twice as thick however, and as noted before was exceptionally difficult to examine prior to the background cancellation via the steel pipe. The ^{241}Am signal was so weak after passing through the tin target, that getting accurate changes in the count rate proved quite a task. The calculated values for lambda are, again, very reasonable.

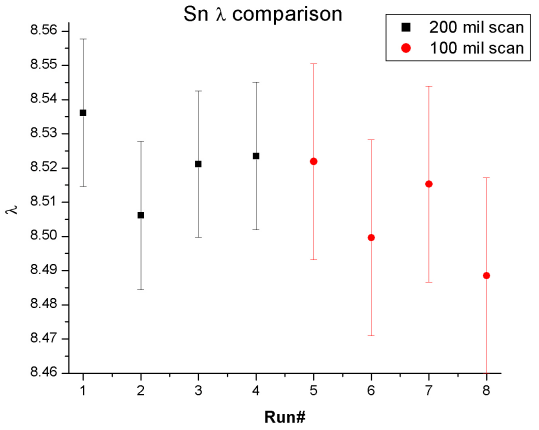

Figure 37 – Calculated lambda values for Sn

Sn Target Thickness

X (mils)	Y (mils)	T (200 mil)	sT (200 mil)	T (100 mil)	sT (100 mil)
-200	-400	23.1233	0.0641	23.1851	0.0715
-100	-400			22.9961	0.0706
0	-400	22.9130	0.0633	22.9523	0.0704
100	-400			22.7371	0.0694
200	-400	22.7275	0.0625	22.9638	0.0704
-300	-300			23.0875	0.0711
-200	-300			23.0911	0.0710
-100	-300			23.0643	0.0709
0	-300			22.9355	0.0703
100	-300			22.9112	0.0702
200	-300			22.8291	0.0699
300	-300			22.6959	0.0693
-400	-200	23.1906	0.0644	23.3817	0.0725
-300	-200			23.2207	0.0717
-200	-200	23.2137	0.0645	23.1300	0.0713
-100	-200			22.9914	0.0706
0	-200	23.1071	0.0641	22.9383	0.0704
100	-200			22.8829	0.0701
200	-200	22.9189	0.0633	22.9192	0.0703
300	-200			22.6787	0.0692
400	-200	22.8840	0.0632	22.9392	0.0704
-400	-100			23.2705	0.0720
-300	-100			23.1962	0.0716
-200	-100			23.2024	0.0716
-100	-100			23.0740	0.0710
0	-100			23.1049	0.0712
100	-100			22.9842	0.0706
200	-100			22.9188	0.0703
300	-100			22.8844	0.0702
400	-100			22.7412	0.0695
-400	0	23.3362	0.0650	23.4825	0.0729
-300	0			23.2904	0.0720
-200	0	23.2633	0.0647	23.2071	0.0716
-100	0			23.1741	0.0715
0	0	23.1053	0.0641	23.1587	0.0714
100	0			23.0521	0.0709
200	0	23.0348	0.0638	22.9315	0.0704
300	0			22.7723	0.0697
400	0	22.8231	0.0629	22.8219	0.0699
-400	100			23.3690	0.0724
-300	100			23.3330	0.0722
-200	100			23.1512	0.0714
-100	100			23.1972	0.0716
0	100			23.1606	0.0714
100	100			23.0383	0.0709
200	100			23.0594	0.0710
300	100			23.0748	0.0710
400	100			22.8768	0.0701
-400	200	23.5345	0.0659	23.4515	0.0728
-300	200			23.2449	0.0718
-200	200	23.3416	0.0650	23.2805	0.0720
-100	200			23.2810	0.0720
0	200	23.0702	0.0639	23.0467	0.0709
100	200			23.1147	0.0712
200	200	23.2065	0.0645	23.1624	0.0714
300	200			22.9609	0.0705
400	200	23.2837	0.0648	23.0620	0.0710
-300	300			23.3657	0.0724
-200	300			23.2766	0.0720
-100	300			23.2649	0.0719
0	300			23.1763	0.0715
100	300			23.1841	0.0715
200	300			23.0057	0.0707
300	300			23.1573	0.0714
-200	400	23.3191	0.0650	23.3464	0.0723
-100	400			23.1329	0.0713
0	400	23.2265	0.0645	23.1638	0.0714
100	400			23.2834	0.0720
200	400	23.2000	0.0645	23.2979	0.0720

Table 6 – Sn Thickness values, 200 mil and 100 mil scans

The data for the tin target, as given in Table 6, shows the difficulty in examining this target. Many of the points in the 200 mil scan differ from those of the 100 mil scan by more than one would wish for. Though overall the two scans again portray the same general makeup of the foil.

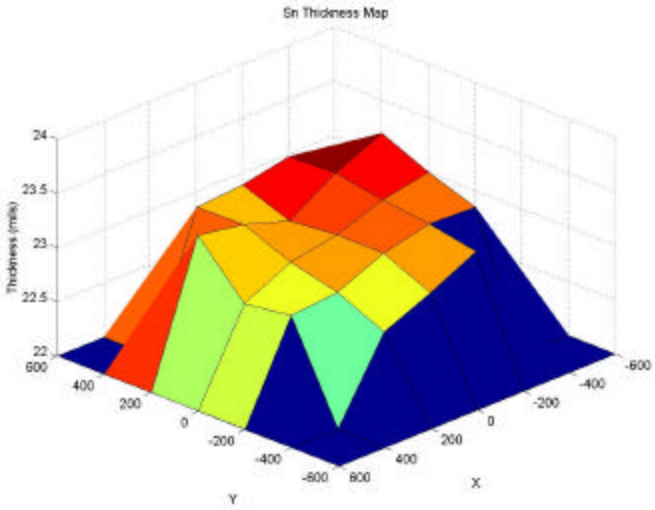

Figure 38 – Sn scan at 200 mils

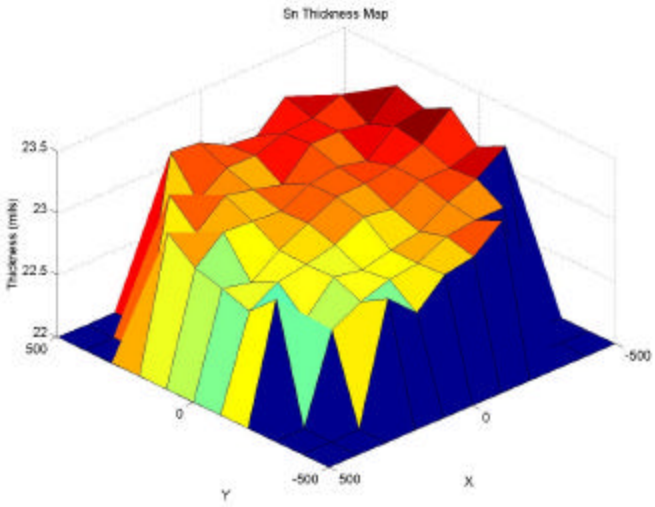

Figure 39 – Sn scan at 100 mils

Both scans show a general gradient in the +Y and -X directions. The 100 mil scan displays a much bumpier image of the target, which should be considered carefully in the data analysis of Primex. The overall gradient of the foil is very clearly shown in the crosscuts through each axis.

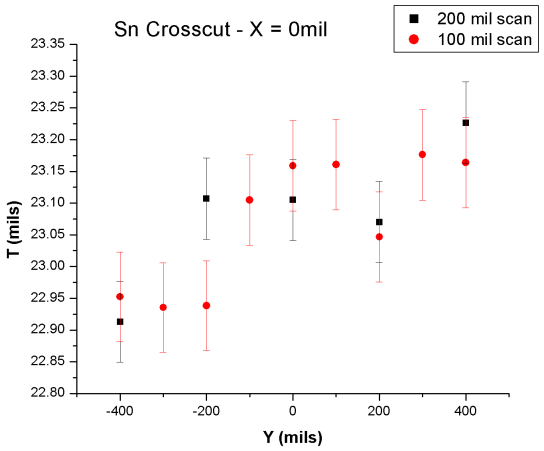

Figure 40 – Crosscut of Sn along Y axis

The 'dip' shown in the Y crosscut at 200 mils is a good example of the 'bumpy' nature of this foil data. How much that point holds up as being accurate is truly left to the reader, mainly the Primex team, to discern. Considering that the two scans produce a very similar result for that point, and the fact that the 200 mil scan is based on three separate measurements of the count rate through the mic points (thus a more accurate value for lambda), I find the data very convincing.

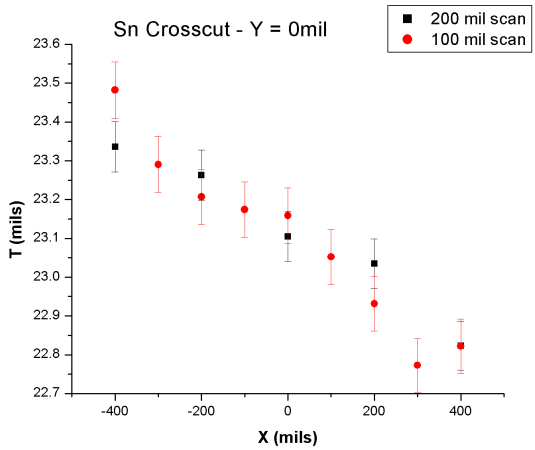

Figure 41 – Crosscut of Sn along X axis

The X crosscut, on the other hand, shows an almost perfect gradient. Achieving such data with such precision, especially with regard to the Sn foil, shows the true success of this project. The ease of the software, and the as of now complete working order of the electronics, allows for the possibility of further studies on these targets once Primex is complete.

XADDIFT Test on HOPG

Given the small percentage variation of these blocks, and the ability to

carefully measure them directly without subsequently altering them, there would seem to be no use for the XADDIFT program here. However, the principle of XADDIFT can be incorporated usefully as a check for uniform density. Given the small, approximately 0.079%, variation in thickness, a large variation in the count rate of the ^{241}Am source through different parts of the block would indicate potential pockets. If the intensity is uniform, within uncertainty and the targets thickness variation, then uniform density can reasonably be assumed.

X	Y	N	s N	ln(N0/N)	X	Y	N	s N	ln(N0/N)
-200	-400	0.08411	0.00016	0.39663	100	0	0.08441	0.00016	0.39313
-100	-400	0.08441	0.00016	0.39312	200	0	0.08415	0.00016	0.39621
0	-400	0.08461	0.00016	0.39070	300	0	0.08423	0.00016	0.39522
100	-400	0.08440	0.00016	0.39329	400	0	0.08436	0.00016	0.39371
200	-400	0.08385	0.00016	0.39983	-400	100	0.08437	0.00016	0.39362
-300	-300	0.08464	0.00016	0.39040	-300	100	0.08483	0.00016	0.38810
-200	-300	0.08416	0.00016	0.39612	-200	100	0.08432	0.00016	0.39416
-100	-300	0.08431	0.00016	0.39430	-100	100	0.08444	0.00016	0.39272
0	-300	0.08429	0.00016	0.39452	0	100	0.08472	0.00016	0.38940
100	-300	0.08417	0.00016	0.39601	100	100	0.08432	0.00016	0.39416
200	-300	0.08450	0.00016	0.39207	200	100	0.08437	0.00016	0.39356
300	-300	0.08413	0.00016	0.39640	300	100	0.08452	0.00016	0.39186
-400	-200	0.08389	0.00016	0.39925	400	100	0.08446	0.00016	0.39252
-300	-200	0.08399	0.00016	0.39811	-400	200	0.08442	0.00016	0.39295
-200	-200	0.08393	0.00016	0.39878	-300	200	0.08472	0.00016	0.38945
-100	-200	0.08418	0.00016	0.39589	-200	200	0.08465	0.00016	0.39022
0	-200	0.08407	0.00016	0.39716	-100	200	0.08419	0.00016	0.39567
100	-200	0.08422	0.00016	0.39535	0	200	0.08447	0.00016	0.39241
200	-200	0.08415	0.00016	0.39619	100	200	0.08445	0.00016	0.39264
300	-200	0.08420	0.00016	0.39560	200	200	0.08440	0.00016	0.39318
400	-200	0.08354	0.00016	0.40349	300	200	0.08459	0.00016	0.39098
-400	-100	0.08412	0.00016	0.39659	400	200	0.08396	0.00016	0.39851
-300	-100	0.08390	0.00016	0.39916	-300	300	0.08450	0.00016	0.39205
-200	-100	0.08381	0.00016	0.40027	-200	300	0.08445	0.00016	0.39265
-100	-100	0.08399	0.00016	0.39816	-100	300	0.08459	0.00016	0.39104
0	-100	0.08418	0.00016	0.39582	0	300	0.08470	0.00016	0.38972
100	-100	0.08404	0.00016	0.39754	100	300	0.08452	0.00016	0.39176
200	-100	0.08438	0.00016	0.39353	200	300	0.08423	0.00016	0.39519
300	-100	0.08395	0.00016	0.39856	300	300	0.08441	0.00016	0.39315
400	-100	0.08388	0.00016	0.39943	-200	400	0.08442	0.00016	0.39304
-400	0	0.08420	0.00016	0.39556	-100	400	0.08474	0.00016	0.38925
-300	0	0.08417	0.00016	0.39591	0	400	0.08449	0.00016	0.39218
-200	0	0.08411	0.00016	0.39673	100	400	0.08483	0.00016	0.38814
-100	0	0.08430	0.00016	0.39442	200	400	0.08402	0.00016	0.39777
0	0	0.08411	0.00016	0.39662					

Table 7 – XADDIFT run on HOPG target II

Since the thickness is, as discussed earlier, the ln(N0/N) term times the x-ray attenuation length lambda (a constant), the percent variation of ln(N0/N) should match the variation in the thickness of the material. We see, however, that with the smallest value being 0.388104, and the largest being 0.403493, the variation is ±1.944%, much larger than the overall variation in thickness. This could indicate pockets of various densities in the material, something which should be further investigated at the conclusion of the beamtime portion of Primex.